

**SERS-BASED BIOSENSING APPLICATIONS AND  
ENANTIOSELECTIVE DISCRIMINATION USING  
GLANCING ANGLE DEPOSITED  
NANOSTRUCTURES**

**SARJANA YADAV**



**DEPARTMENT OF PHYSICS**

**INDIAN INSTITUTE OF TECHNOLOGY DELHI**

**AUGUST 2024**

**© Indian Institute of Technology Delhi (IITD), New Delhi, 2024**

**All rights reserved.**

**SERS-BASED BIOSENSING APPLICATIONS AND  
ENANTIOSELECTIVE DISCRIMINATION USING  
GLANCING ANGLE DEPOSITED  
NANOSTRUCTURES**

by

**SARJANA YADAV**

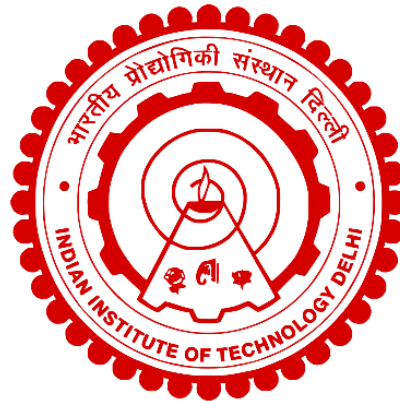
**Department of physics**

**Submitted**

**in fulfillment of the requirements of the degree of**

**Doctor of Philosophy**

**to the**



**INDIAN INSTITUTE OF TECHNOLOGY DELHI**

**AUGUST 2024**

## CERTIFICATE

---

This is to certify that the thesis entitled “*SERS-based biosensing applications and enantioselective discrimination using glancing angle deposited nanostructures,*” submitted by **Ms. Sarjana Yadav** to the Indian Institute of Technology Delhi, is worthy of consideration for the award of the degree of **Doctor of Philosophy** and is a Bonafide record of the research work carried out by her under my supervision. The contents of this thesis, in full or in parts, have not been submitted to any other Institute or University for the award of any degree or diploma.

Place: New Delhi

Date: 02-08-2024



**Prof. J. P. Singh**

Department of Physics  
Indian Institute of Technology Delhi  
New Delhi-110016  
India

## ACKNOWLEDGEMENT

---

I would like to express my sincere gratitude to my thesis supervisor, my family, my friends, well-wishers and the almighty to successfully accomplish my doctoral thesis.

First and foremost, I would like to thank the omnipresent God, for the immeasurable blessings and guidance throughout the journey, for bestowing upon me the wisdom for the right path.

This work would have never reached this form without the guidance of my supervisor, Prof. J.P. Singh. I immensely thank him for his constant technical, moral and emotional support throughout my Ph.D. journey. His guidance, patience and constant selfless support by sharing his expertise and devoting his valuable time kept me motivated throughout my Ph.D. years to aspire for better. I'm indebted to him for giving me intellectual freedom for work, supporting flexible working hours, encouraging me to attend conferences and other scientific events in and outside the institute, engaging me in new ideas, and always pushing for the highest quality of work in all my endeavors. His positive work attitude has always encouraged me to do high-quality research work.

I further acknowledge the University Grant Commission (UGC) and IIT Delhi for all the financial support throughout the Ph.D. journey. I thank the nanoscale research facility (NRF) and central research facility (CRF), IIT Delhi, for providing all the experimental and characterization facilities to accomplish my research work. I heartfully thank IIT Delhi for the healthy, comfortable, and friendly work ambience.

I would then like to thank my SRC members Prof. D.S. Mehta, Prof. Kedar Khare, and Dr. Sandeep Jha for their valuable inputs at different stages of my Ph.D. The discussions with my SRC members have been really very fruitful.

I am very thankful to be a part of GLAD and nano-CVD lab. I want to express my immense gratitude to all the fellow members of the group. Firstly, the seniors- Dr. Parul Raturi, Dr. Shashank Gahlaut, Dr. Rizwin, Dr. Pinki and Dr. Yogita for their guidance and helping me to evolve with the basics of research when I was naive to the lab. Then I would like to thank my fellow batchmates-cum-friends at the lab -Mr. Jamal Khan

and Ms. Jyoti Yadav for the research related help and discussions. I thank them for such wonderful memorable moments in the lab and at the conferences we did together. I would then like to express my thanks to Ms. Sneha Senapati for being such a nice friend and collaborator since my very initial Ph.D. days. Her presence made my scientific visits to the National AIDS Research Institute (NARI), Pune, really comfortable and memorable. I would then extend my gratitude to the juniors at the lab-Mr. Arvind, Mr. Sidharth, Ms. Vidhya CM, Mr. Lakshay Bhardwaj, Mr. Shivam Singh, Mr. Debottam, and Ms. Prerna for all the technical help and support as well as creating such a joyful environment inside and outside the lab. A special thanks to Ms. Jyoti (technical lab assistant) for her professional and friendly support since my Ph.D. beginning. All of these lab mates have created a home-like environment at the lab.

I have an extended group of friends who have been my support system throughout the journey. I want to express my heartfelt thanks to Mr. Varun Arora for his kind support and motivation at professional as well as personal levels throughout the Ph.D. years, for patiently listening to me and giving different new ideas and solutions. I am fortunate enough to be blessed with friends-Ms. Surbhi Singh, Mr. Pravin Rawat, Ms. Sumegha Gupta, Ms. Pankhuri Gupta, Mr. Tahir Ahmad and Mr. Prakash Joshi. I thank them for being by my side, for their valuable ideas, discussions and emotional support in all ups and downs all along the journey.

It will be unfair on my part if I don't acknowledge my colleagues at my recent workplace (N.R.E.C. College, Khurja, U.P.). I express my sincere thanks to my colleagues-cum-friends- Ms. Jyoti Yadav, Ms. Neha Sharma, Mr. Aashish Kumar, Mr. Sumit Kumar, and Ms. Kirti Agarwal for their immense support in helping me to manage my responsibilities at my work palace and research lab at IIT. Without their support, it would have been almost impossible to finish my Ph.D. work, especially during its last stages.

My thesis is incomplete without expressing my sincere gratitude to my father (Dr. Shyama Prasad Yadav), mother (Mrs. Vidya Yadav), and siblings (Dr. Smriti, Mr. Yash, and Ms. Samiksha). I thank them for their love, blessings, prayers, care, and wishes. Without their support, I could have never accomplished whatever I have today.

Their consistent faith and patience have encouraged me to pursue my dreams with flying colors.

Finally, I am grateful to each and every person who has directly or indirectly contributed to and supported me in completing this thesis.

**Sarjana Yadav**

## ABSTRACT

---

Surface-enhanced Raman scattering (SERS) is the enormous amplification of the Raman signals from analytes, by several orders of magnitude, when the molecule is adsorbed on the metal colloidal nanoparticles or the roughened metal surface. The detection of the analyte molecules even at a single-molecule level can be done by using the SERS technique which has therefore found a huge practical application. SERS has found its applications in various aspects, including the trace chemical detection such as dyes, explosive detection, food additives, pesticides, as well as in the bioanalysis, biomolecules detection, cancer diagnosis, medical diagnosis and the in-vivo molecular probing in the live cells. SERS substrates are the nanostructured platform that supports the plasmon resonance and hence amplifies Raman signals. These may be of random morphology or ordered SERS substrates. Most of the research has been carried out using the random morphology SERS substrates (such as metallic nanoparticles, roughened electrodes etc.) due to its ease of preparation. However, these substrates due to their lack of uniformity possess severe issues with the uniformity of the results therefore, these substrates cannot be completely employed as one of the routine analytical techniques. Glancing angle deposition (GLAD) is one of the physical vapor deposition techniques in which the gaseous flow of the depositing atoms gets impinged on the substrate in a vacuum environment at a given oblique angle resulting in a columnar morphology of the deposited film as a result of the shadowing effect. The GLAD technique is considered as better than other growth methods especially the ones resulting in random morphology in the terms of ease of fabrication of the nanostructures due to controlled shape, size and the column spacing in a single step. Moreover, the nanostructures grown by this technique possess high porosity, high surface to the volume ratio, uniformity and crystallinity making it one of the most suitable techniques for the sensing applications. Therefore, GLAD has emerged as one of the versatile techniques to fabricate nanostructures with a wide range of material of varying sizes and morphologies. Highly reproducible and uniform SERS substrates with different morphologies with a batch-to-batch and sample to sample reproducibility that have a SERS signal variation of less than 10% can be fabricated using this GLAD technique. Recently, silver nanostructures of different morphologies grown using GLAD have

attracted a significant attention due to their promising applications in the surface plasmon based studies and for fabrication of the highly sensitive SERS substrates with a very high enhancement.

The above background forms a basis of the objectives of the present thesis. The central objective of the thesis work is to study the Ag nanostructured SERS substrates fabricated using GLAD for their potential application in biosensing and biomedicine. SERS being molecular fingerprint detection technique also comes with certain serious limitations such as requirement of adequate SERS substrate, its ultra-high sensitivity, reproducibility of the results, background interference, dilution of analyte with other matrix and its limited ability for detection only (inability of separation). We have tried to address and overcome all these limitations in this thesis along with a future perspective of employing SERS for on-field detection. Different types of new SERS substrates have been fabricated by GLAD. We have developed a novel highly sensitive Ag nanorods (AgNRs) SERS platform for HIV-1 viral load quantification and determination of disease prognosis without using any external reagent. Once the HIV-1 signature peaks library was established, we used the developed platform for HIV-1 clinical sample detection. Further, Magnetic- SERS sensing of hemozoin was performed which is a biomarker of malaria for rapid and early malaria diagnosis. This was extended by magnetic field augmented ultrathin layer chromatography- SERS detection and separation of hemozoin from bacterial mixture. Finally, we have employed GLAD for Ultrasensitive chiral SERS substrates for label free enantioselective discrimination. 2 types of novel chiral SERS substrates were fabricated using GLAD for ultrasensitive chiral SERS discrimination.

In resource limited settings, a cost-effective point-of-care diagnostic testing possessing the characteristics of detecting the minimum viral load of a malady like HIV acquired immune deficiency syndrome AIDS is a pressing priority. A highly optimized AgNRs array, fabricated using GLAD technique was used as SERS substrate. Distinct signature peaks for varying concentrations ( $10^2$  to  $10^6$  copies/ml) were identified in five different HIV-1 subtypes (A, B, C, D, and CRF02\_AG). Binding of viruses directly with Ag nanorods without using antibodies or intermediate reagents is shown. The purified viruses were spiked in water and healthy plasma to capture pure HIV-1 peaks. Distinct

peaks were also captured for the X4 and R5 tropic strains suggesting tropism-based detection. The above data was further confirmed and analyzed statistically using a multivariate tool. Thus, the present study indicates the ability of the SERS platform to detect and differentiate the HIV-1 virus implying its further validation using clinical specimens and isolates. We have further developed a novel, rapid and field-deployable method using SERS for detection and prognosis of HIV positive clinical samples, in seven different viral load ranges varying between 200 to 1 million copies/ml. A relationship between the increasing and decreasing intensity peaks of HIV-1 was also established for quantitation efficacy of the handheld tool. Three different types of SERS substrates: single arm Ag nanorods, double arm Ag nanorods and Au sputtered single arm Ag nanorods were used and the obtained data was compared for the three substrates. It was demonstrated that maximum enhancement was obtained for Au sputtered Ag nanorods. Rigorous coupled wave analysis (RCWA) simulations were performed to study the 'hotspots' in three different SERS substrates. Further, to explore the utility of our platform and to differentiate between the clade specific X4 and R5 tropism, their corresponding-SERS spectra were studied using HIV-1 strains belonging to four different HIV-1 subtypes (A, B, C and D) which showed a clear distinction, implying the usefulness of the platform in understanding the disease prognosis. Statistical analysis of the obtained SERS spectra using principal component analysis (PCA) showed good agreement with the experimental results, confirming the ability of SERS platform to quantify HIV-1 viral load and distinguish HIV-1 strains on the basis of their SERS spectra.

We have further reported detection of hemozoin, a metabolic byproduct of malaria parasite exhibiting paramagnetic properties using magnetic SERS (M-SERS). The SERS active silver nanorods were deposited over neodymium magnetic substrates (0.3T) kept at 120K temperature using GLAD technique. Magnetic field augmented SERS measurements were performed for hemozoin on these M-SERS substrates and AgNRs deposited over glass (conventional SERS) substrates in presence of an external magnetic field (0.3 T). The SERS signal intensity was found to be enhanced by ten-fold compared to the measurements performed on the conventional SERS substrates in the absence of any magnetic field. The presence of high spin trivalent iron in hemozoin

structure led the magnetic field induced agglomeration of these molecules in vicinity of the electromagnetic ‘hotspots’ available on the SERS substrates which was confirmed by running RCWA based simulations. These interactions lead to higher enhancement of vibrational modes of the porphine group directly linked to iron. The limit of detection of hemozoin for M-SERS was obtained as low as  $10^{-11}$  M ( $< 10$  parasites/ $\mu$ l) which can be employed for early-stage malaria detection. Since, malaria is considered as one the most widespread disease with highest possibility of co-infection at all levels of the disease prognosis, rapid detection and discrimination of malaria from other co-infections remains a challenge. We have therefore extended the detection of hemozoin with the development of a label free, rapid and highly sensitive magnetic field augmented ultra-thin layer chromatography (UTLC) combined with SERS method for detection and separation of hemozoin, a malaria biomarker from bacterial mixture. Highly optimized silver nanorods based chip fabricated using GLAD is explored for the UTLC-SERS separation. Magnetic nature of hemozoin possessing iron at its centre increasing its ability to flow towards the magnet has been exploited for its separation from a mixture of *P. aeruginosa* (Gram-negative) and *S. aureus* (Gram-positive) by allocating a 0.6 T magnet over the UTLC flow setup. The SERS data was taken along the solvent front from the mixture loaded point up to a distance of 13 mm at a regular distance of 1 mm after the UTLC flow. Due to magnetic environment, the migrated solvent front with distance  $> 8$  mm showed majorly presence of hemozoin. However the flow of the 2 bacteria remained constricted to a distance of 4 mm - 6 mm strongly separating the mixture with slight indications of separation of *P. aeruginosa* and *S. aureus*. Further, staining of hemozoin, *P. aeruginosa* and *S. aureus* was done using methylene blue, acridine orange and rhodamine 6G respectively and the separation was confirmed. We therefore established a novel technique capable of separating small amounts of analytes aiding in the removal of co-infections from the disease at a very early stage with high a specificity and sensitivity.

Chirality is one of the most important characteristics of the chiral materials with a very important role in biomedicine. Most of the biologically active compounds such as amino acids, peptides, sugars, proteins, *etc.* as well as certain important modern drugs possess chirality. Although the enantiomers of a given molecule have similar

physicochemical properties, they exhibit totally different physiological effects in reference of their biological activity, pharmacological actions and toxicity. Hence, detection as well the discrimination of these chiral molecules plays a very crucial role specially from application point of concern. We have fabricated plasmonic chiral Ag nanostructures using glancing angle deposition (GLAD) technique with strong chiroptic response. GLAD fabricated chiral Ag nanohelices have been explored for label free enantioselective SERS discrimination. 3 different biologically significant enantiomers (DOPA, cystine and tartaric acid) with entirely different chemical features have been successfully differentiated. The homochiral analyte showed distinct and enhanced affinity towards the substrate of homogeneous handedness. Relative intensities of certain specific peaks changed depending on the variations in the enantiomeric environment. The LOD was calculated as  $\sim 10^{-12}$  M for each of the analyte. The distinction mechanism is explained by performing finite difference time domain (FDTD) simulations by studying the local field 'hotspot' distribution in case of each of the plasmonic chiral Ag substrate. Our unique chiral Ag nanostructures allows an effective chiral plasmon excitations in the vicinity of their local fields. Additionally, difference in behaviour of each of the analyte was observed towards a specific chiral substrate which could be clearly explained by the manifestation of the charge transfer (CT) mechanism. Theoretical density functional theory (DFT) calculations were performed in order to get insights into the charge transfer process. The HOMO and LUMO energy levels of each of each of the analyte has been calculated separately and its gap from the Ag fermi level has been determined. We infer that the direction of the CT from Ag to analytes are different in the varying enantiomeric conditions. Therefore, the CT process in combination with the EM mechanism highly magnifies the difference between SERS spectra of 2 enantiomers of a given molecule. Hence, we establish an easy ligand free SERS enantioselective discrimination which may be of huge significance in the fields of chiral separation.

## सारांश

सतह-संवर्धित रमन प्रकीर्णन (SERS) विश्लेष्य पदार्थों से रमन संकेतों का बहुत बड़ा प्रवर्धन है, कई क्रमों के परिमाण द्वारा, जब अणु धातु कोलाइडल नैनोकणों या खुरदरी धातु की सतह पर अवशोषित होता है। एकल-अणु स्तर पर भी विश्लेष्य अणुओं का पता लगाना SERS तकनीक का उपयोग करके किया जा सकता है, जिसने इसलिए एक विशाल व्यावहारिक अनुप्रयोग पाया है। SERS ने विभिन्न पहलुओं में अपने अनुप्रयोग पाए हैं, जिसमें डाई, विस्फोटक पहचान, खाद्य योजक, कीटनाशक जैसे ट्रेस रासायनिक पहचान, साथ ही साथ बायोएनालिसिस, बायोमोलेक्यूल्स पहचान, कैंसर निदान, चिकित्सा निदान और जीवित कोशिकाओं में इन-विवो आणविक जांच शामिल है। SERS सबस्ट्रेट नैनोस्ट्रक्चर्ड प्लेटफॉर्म हैं जो प्लाज़्मोन प्रतिध्वनि का समर्थन करते हैं और इसलिए रमन संकेतों को बढ़ाते हैं। ये यादृच्छिक आकारिकी या क्रमबद्ध SERS सबस्ट्रेट हो सकते हैं। अधिकांश शोध यादृच्छिक आकारिकी SERS सबस्ट्रेट (जैसे धातु नैनोकण, खुरदरे इलेक्ट्रोड आदि) का उपयोग करके किए गए हैं क्योंकि इसे तैयार करना आसान है। हालांकि, इन सबस्ट्रेट्स में एकरूपता की कमी के कारण परिणामों की एकरूपता के साथ गंभीर मुद्दे हैं, इसलिए इन सबस्ट्रेट्स को नियमित विश्लेषणात्मक तकनीकों में से एक के रूप में पूरी तरह से नियोजित नहीं किया जा सकता है। ग्लेसिंग एंगल डिपोजिशन (GLAD) भौतिक वाष्प जमाव तकनीकों में से एक है जिसमें जमा करने वाले परमाणुओं का गैसीय प्रवाह एक निश्चित तिरछे कोण पर वैक्यूम वातावरण में सबस्ट्रेट पर टकराता है, जिसके परिणामस्वरूप छाया प्रभाव के परिणामस्वरूप जमा फिल्म की स्तंभाकार आकृति बनती है। GLAD तकनीक को अन्य विकास विधियों की तुलना में बेहतर माना जाता है, खासकर वे जो एक ही चरण में नियंत्रित आकार, आकार और स्तंभ रिक्ति के कारण नैनोस्ट्रक्चर के निर्माण में आसानी के मामले में यादृच्छिक आकृति विज्ञान का परिणाम देते हैं। इसके अलावा, इस तकनीक द्वारा विकसित नैनोस्ट्रक्चर में उच्च छिद्रता, उच्च सतह से आयतन अनुपात, एकरूपता और क्रिस्टलीयता होती है जो इसे संवेदन अनुप्रयोगों के लिए सबसे उपयुक्त तकनीकों में से एक बनाती है। इसलिए, GLAD विभिन्न आकारों और आकृति विज्ञान की सामग्री की एक विस्तृत श्रृंखला के साथ नैनोस्ट्रक्चर बनाने के लिए बहुमुखी तकनीकों में से एक के रूप में उभरा है। बैच-टू-बैच और सैपल-टू-सैपल प्रजनन क्षमता वाले विभिन्न आकारिकी वाले अत्यधिक पुनरुत्पादनीय और समान SERS सबस्ट्रेट्स जिनमें SERS सिग्नल में 10% से कम भिन्नता होती है, इस GLAD तकनीक का उपयोग करके बनाए जा सकते हैं। हाल ही में, GLAD का उपयोग करके उगाए गए विभिन्न आकारिकी के सिल्वर नैनोस्ट्रक्चर ने सतह प्लाज़्मोन आधारित अध्ययनों में उनके आशाजनक अनुप्रयोगों और बहुत उच्च वृद्धि के साथ अत्यधिक संवेदनशील SERS सबस्ट्रेट्स के निर्माण के कारण महत्वपूर्ण ध्यान आकर्षित किया है।

उपर्युक्त पृष्ठभूमि वर्तमान थीसिस के उद्देश्यों का आधार बनती है। थीसिस कार्य का केंद्रीय उद्देश्य बायोसेंसिंग और बायोमेडिसिन में उनके संभावित अनुप्रयोग के लिए GLAD का उपयोग करके निर्मित  $Ag$  नैनोस्ट्रक्चर वाले SERS सबस्ट्रेट्स का अध्ययन करना है। SERS आणविक फिंगरप्रिंट पहचान तकनीक होने के कारण कुछ गंभीर सीमाएँ

भी लेकर आती है हमने इस थीसिस में इन सभी सीमाओं को संबोधित करने और दूर करने का प्रयास किया है, साथ ही ऑन-फील्ड डिटेक्शन के लिए SERS को नियोजित करने के भविष्य के परिप्रेक्ष्य के साथ। GLAD द्वारा विभिन्न प्रकार के नए SERS सबस्ट्रेट बनाए गए हैं। हमने HIV-1 वायरल लोड क्वांटिफिकेशन और किसी बाहरी अभिकर्मक का उपयोग किए बिना रोग के निदान के निर्धारण के लिए एक नया अत्यधिक संवेदनशील Ag नैनोरोड्स (AgNRs) SERS प्लेटफॉर्म विकसित किया है। एक बार HIV-1 सिग्नेचर पीक्स लाइब्रेरी स्थापित हो जाने के बाद, हमने HIV-1 क्लिनिकल सैंपल डिटेक्शन के लिए विकसित प्लेटफॉर्म का उपयोग किया। इसके अलावा, हेमोज़ोइन की मैग्नेटिक-SERS सेंसिंग की गई, जो मलेरिया के तेजी से और शुरुआती निदान के लिए मलेरिया का बायोमार्कर है। इसे मैग्नेटिक फील्ड ऑगमेंटेड अल्ट्राथिन लेयर क्रोमेटोग्राफी- SERS डिटेक्शन और हेमोज़ोइन को बैक्टीरियल मिश्रण से अलग करके बढ़ाया गया। अंत में, हमने लेबल मुक्त एनेंटियोसेलेक्टिव भेदभाव के लिए अल्ट्रासेंसिटिव चिरल SERS सबस्ट्रेट के लिए GLAD को नियोजित किया है। अल्ट्रासेंसिटिव चिरल SERS भेदभाव के लिए GLAD का उपयोग करके 2 प्रकार के नए चिरल SERS सबस्ट्रेट बनाए गए। सीमित संसाधनों वाली स्थितियों में, एचआईवी एकायर्ड इम्यून डेफिसिएंसी सिंड्रोम एड्स जैसी बीमारी के न्यूनतम वायरल लोड का पता लगाने की विशेषताओं वाला एक लागत प्रभावी पॉइंट-ऑफ-केयर डायग्नोस्टिक परीक्षण एक महत्वपूर्ण प्राथमिकता है। GLAD तकनीक का उपयोग करके निर्मित एक अत्यधिक अनुकूलित AgNRs सरणी का उपयोग SERS सबस्ट्रेट के रूप में किया गया था। अलग-अलग सांद्रता (102 से 106 प्रतियाँ/एमएल) के लिए अलग-अलग सिग्नेचर पीक की पहचान पाँच अलग-अलग HIV-1 उपप्रकारों (A, B, C, D, और CRF02\_AG) में की गई। एंटीबॉडी या इंटरमीडिएट अभिकर्मकों का उपयोग किए बिना सीधे Ag नैनोरोड्स के साथ वायरस को बांधना दिखाया गया है। शुद्ध किए गए वायरस को शुद्ध एचआईवी-1 चोटियों को पकड़ने के लिए पानी और स्वस्थ प्लाज्मा में मिलाया गया था। ट्रॉपिज़्म-आधारित पता लगाने का सुझाव देते हुए एक्स4 और आर5 ट्रॉपिक उपभेदों के लिए अलग-अलग चोटियों को भी पकड़ा गया था। उपरोक्त डेटा की आगे पुष्टि की गई और एक बहुभिन्नरूपी उपकरण का उपयोग करके सांख्यिकीय रूप से विश्लेषण किया गया। इस प्रकार, वर्तमान अध्ययन एचआईवी-1 वायरस का पता लगाने और उसे अलग करने के लिए एसईआरएस प्लेटफॉर्म की क्षमता को इंगित करता है, जिसका तात्पर्य नैदानिक नमूनों और आइसोलेट्स का उपयोग करके इसके आगे के सत्यापन से है। हमने 200 से 1 मिलियन प्रतियों/एमएल के बीच अलग-अलग सात अलग-अलग वायरल लोड श्रेणियों में एचआईवी पॉजिटिव नैदानिक नमूनों का पता लगाने और निदान के लिए एसईआरएस का उपयोग करके एक उपन्यास, तेज़ और क्षेत्र-तैनाती विधि विकसित की है। हैंडहेल्ड टूल की मात्रा निर्धारण प्रभावकारिता के लिए एचआईवी-1 की यह प्रदर्शित किया गया कि Au स्प्टरेड Ag नैनोरोड्स के लिए अधिकतम वृद्धि प्राप्त की गई थी। तीन अलग-अलग SERS सबस्ट्रेट्स में 'हॉटस्पॉट' का अध्ययन करने के लिए कठोर युग्मित तरंग विश्लेषण (RCWA) सिमुलेशन किए गए थे। इसके अलावा, हमारे प्लेटफॉर्म की उपयोगिता का पता लगाने और क्लैड विशिष्ट X4 और R5 ट्रॉपिज़्म के बीच अंतर करने के लिए, उनके संबंधित SERS स्पेक्ट्रा का अध्ययन चार अलग-अलग HIV-1 उपप्रकारों (A, B, C और D) से संबंधित HIV-1 उपभेदों का उपयोग करके किया गया, जिसमें स्पष्ट अंतर दिखा, जिससे रोग के निदान को समझने में प्लेटफॉर्म की उपयोगिता का संकेत मिला। प्रमुख घटक विश्लेषण (PCA)

का उपयोग करके प्राप्त SERS स्पेक्ट्रा के सांख्यिकीय विश्लेषण ने प्रयोगात्मक परिणामों के साथ अच्छा समझौता दिखाया, जिससे SERS प्लेटफॉर्म की HIV-1 वायरल लोड को मापने और उनके SERS स्पेक्ट्रा के आधार पर HIV-1 उपभेदों को अलग करने की क्षमता की पुष्टि हुई। SERS सक्रिय सिल्वर नैनोरोड्स को GLAD तकनीक का उपयोग करके 120K तापमान पर रखे गए नियोजिमियम चुंबकीय सबस्ट्रेट (0.3T) पर जमा किया गया। इन M-SERS सबस्ट्रेट पर हेमोज़ोइन के लिए चुंबकीय क्षेत्र संवर्धित SERS माप किए गए और बाहरी चुंबकीय क्षेत्र (0.3 T) की उपस्थिति में ग्लास (पारंपरिक SERS) सबस्ट्रेट पर AgNRs जमा किए गए। किसी भी चुंबकीय क्षेत्र की अनुपस्थिति में पारंपरिक SERS सबस्ट्रेट पर किए गए मापों की तुलना में SERS सिग्नल की तीव्रता दस गुना बढ़ गई। हेमोज़ोइन संरचना में उच्च स्पिन त्रिसंयोजक लोहे की उपस्थिति ने SERS सबस्ट्रेट पर उपलब्ध विद्युत चुंबकीय 'हॉटस्पॉट' के आसपास इन अणुओं के चुंबकीय क्षेत्र प्रेरित समूहन को जन्म दिया, जिसकी पुष्टि RCWA आधारित सिमुलेशन चलाकर की गई। ये अंतःक्रियाएँ सीधे लोहे से जुड़े पॉर्फिन समूह के कंपन मोड में उच्च वृद्धि की ओर ले जाती हैं। एम-एसईआरएस के लिए हीमोज़ोइन की पहचान की सीमा 10-11 एम (<10 परजीवी/ $\mu\text{l}$ ) जितनी कम पाई गई, जिसका उपयोग मलेरिया की शुरुआती अवस्था में पहचान के लिए किया जा सकता है। चूंकि, मलेरिया को सबसे व्यापक बीमारी माना जाता है, जिसमें रोग निदान के सभी स्तरों पर सह-संक्रमण की सबसे अधिक संभावना होती है, इसलिए मलेरिया का अन्य सह-संक्रमणों से तेजी से पता लगाना और उसका भेदभाव करना एक चुनौती बनी हुई है। इसलिए हमने हीमोज़ोइन की पहचान को एक लेबल मुक्त, तेज और अत्यधिक संवेदनशील चुंबकीय क्षेत्र संवर्धित अल्ट्रा-थिन लेयर क्रोमैटोग्राफी (UTLC) के विकास के साथ आगे बढ़ाया है, जिसे बैक्टीरिया के मिश्रण से मलेरिया बायोमार्कर हीमोज़ोइन का पता लगाने और अलग करने के लिए SERS विधि के साथ जोड़ा गया है। UTLC-SERS पृथक्करण के लिए GLAD का उपयोग करके निर्मित अत्यधिक अनुकूलित सिल्वर नैनोरोड्स आधारित चिप की खोज की गई है। हेमोज़ोइन की चुंबकीय प्रकृति, जिसके केंद्र में लोहा होता है, चुंबक की ओर बहने की इसकी क्षमता को बढ़ाती है, यूटीएलसी प्रवाह सेटअप पर 0.6 टी चुंबक आवंटित करके पी. एरुगिनोसा (ग्राम-नेगेटिव) और एस. ऑरियस (ग्राम-पॉजिटिव) के मिश्रण से इसे अलग करने के लिए उपयोग किया गया है। यूटीएलसी प्रवाह के बाद 1 मिमी की नियमित दूरी पर 13 मिमी की दूरी तक मिश्रण लोड किए गए बिंदु से सॉल्वेंट फ्रंट के साथ SERS डेटा लिया गया था। चुंबकीय वातावरण के कारण, 8 मिमी से अधिक दूरी वाले माइग्रेटेड सॉल्वेंट फ्रंट में हेमोज़ोइन की प्रमुख उपस्थिति देखी गई। हालांकि 2 बैक्टीरिया का प्रवाह 4 मिमी - 6 मिमी की दूरी तक सीमित रहा इसलिए हमने एक नई तकनीक विकसित की है जो विश्लेषकों की छोटी मात्रा को अलग करने में सक्षम है, जो उच्च विशिष्टता और संवेदनशीलता के साथ रोग से सह-संक्रमण को बहुत प्रारंभिक चरण में हटाने में सहायता करती है।

चिरैलिटी चिरल पदार्थों की सबसे महत्वपूर्ण विशेषताओं में से एक है, जिसकी बायोमेडिसिन में बहुत महत्वपूर्ण भूमिका है। अधिकांश जैविक रूप से सक्रिय यौगिक जैसे कि अमीनो एसिड, पेप्टाइड्स, शर्करा, प्रोटीन, आदि के साथ-साथ कुछ महत्वपूर्ण आधुनिक दवाओं में भी चिरैलिटी होती है। यद्यपि किसी दिए गए अणु के एनेंटीओमर में

समान भौतिक गुण होते हैं, लेकिन वे अपनी जैविक गतिविधि, औषधीय क्रियाओं और विषाक्तता के संदर्भ में पूरी तरह से अलग शारीरिक प्रभाव प्रदर्शित करते हैं। इसलिए, इन चिरल अणुओं का पता लगाना और उनका भेदभाव करना विशेष रूप से चिंता के अनुप्रयोग बिंदु से बहुत महत्वपूर्ण भूमिका निभाता है। हमने मजबूत चिरौष्टिक प्रतिक्रिया के साथ ग्लेंसिंग एंगल डिपोजिशन (GLAD) तकनीक का उपयोग करके प्लास्मोनिक चिरल Ag नैनोस्ट्रक्चर का निर्माण किया है। लेबल मुक्त एनेंटियोसेलेक्टिव SERS भेदभाव के लिए GLAD निर्मित चिरल Ag नैनोहेलिस का पता लगाया गया है। पूरी तरह से अलग रासायनिक विशेषताओं वाले 3 अलग-अलग जैविक रूप से महत्वपूर्ण एनेंटिओमर (DOPA, सिस्टीन और टार्टरिक एसिड) को सफलतापूर्वक विभेदित किया गया है। होमोचिरल एनालाइट ने सजातीय हाथ के सबस्ट्रेट के प्रति अलग और बढ़ी हुई आत्मीयता दिखाई। कुछ विशिष्ट चोटियों की सापेक्ष तीव्रता एनेंटिओमेरिक वातावरण में भिन्नता के आधार पर बदल गई। प्रत्येक विश्लेषक के लिए LOD की गणना ~ 10-12 M के रूप में की गई थी। प्रत्येक प्लाज़्मोनिक चिरल Ag सबस्ट्रेट के मामले में स्थानीय क्षेत्र 'हॉटस्पॉट' वितरण का अध्ययन करके परिमित अंतर समय डोमेन (FDTD) सिमुलेशन करके भेद तंत्र को समझाया गया है। हमारे अद्वितीय चिरल Ag नैनोस्ट्रक्चर उनके स्थानीय क्षेत्रों के आसपास के क्षेत्र में एक प्रभावी चिरल प्लाज़्मोन उत्तेजना की अनुमति देते हैं। इसके अतिरिक्त, प्रत्येक विश्लेषक के व्यवहार में एक विशिष्ट चिरल सबस्ट्रेट के प्रति अंतर देखा गया था जिसे चार्ज ट्रांसफर (CT) तंत्र की अभिव्यक्ति द्वारा स्पष्ट रूप से समझाया जा सकता है। चार्ज ट्रांसफर प्रक्रिया में अंतर्दृष्टि प्राप्त करने के लिए सैद्धांतिक घनत्व कार्यात्मक सिद्धांत (DFT) गणना की गई थी। प्रत्येक विश्लेषक के HOMO और LUMO ऊर्जा स्तरों की अलग-अलग गणना की गई है और Ag फर्मी स्तर से इसका अंतर निर्धारित किया गया है। हम अनुमान लगाते हैं कि Ag से एनालाइट्स तक CT की दिशा अलग-अलग एनेंटिओमेरिक स्थितियों में अलग-अलग होती है। इसलिए, EM तंत्र के साथ संयोजन में CT प्रक्रिया किसी दिए गए अणु के 2 एनेंटिओमर के SERS स्पेक्ट्रा के बीच अंतर को अत्यधिक बढ़ा देती है। इसलिए, हम एक आसान लिगैंड मुक्त SERS एनेंटिओसेलेक्टिव भेदभाव स्थापित करते हैं जो कि चिरल पृथक्करण के क्षेत्रों में बहुत महत्वपूर्ण हो सकता है।

# CONTENT

---

Certificate.....	i
Acknowledgements.....	ii
Abstract.....	v
सारांश .....	x
Table of contents.....	xiv
List of Figures .....	xix
List of Tables .....	xxviii
Symbols.....	xxx
Abbreviations.....	xxxi
<b>CHAPTER 1: INTRODUCTION.....</b>	<b>1</b>
1.1 Introduction.....	2
1.3. Surface enhanced Raman spectroscopy .....	9
1.4. SERS substrates .....	17
1.5. Glancing angle deposition (GLAD).....	20
1.5.1. Fabrication GLAD technique-based nanostructures.....	21
1.6. Silver columnar optical properties and its SERS performance.....	26
1.7. Chirality and SERS based chiral detection .....	28
1.8. Objectives of the present thesis.....	31
1.9. Thesis overview .....	32
<b>CHAPTER 2: EXPERIMENTAL AND CHARACTERIZATION TECHNIQUES, SIMULATION METHODOLOGY AND STATISTICAL CLASSIFICATION .....</b>	<b>34</b>
2.1. Glancing angle deposition.....	35
2.1.1. Homemade GLAD setup with fixed substrate holder .....	36
2.1.2. Advanced GLAD system with variable $\alpha$ and $\phi$ .....	37
2.1.3. Substrate packaging unit .....	38
2.2. X -Ray diffraction .....	39
2.3. Field emission scanning electron microscopy (FESEM).....	40
2.4. Transmission electron microscope (TEM).....	41
2.5. Atomic force microscopy (AFM) .....	42

2.6. Micro-Raman spectrometer .....	43
2.7. Simulations methods and statistical tools .....	45
2.7.1. Finite difference time domain (FDTD) models and simulation methodology .....	45
2.7.2. Rigorous coupled wave analysis (RCWA) simulations and modeling.....	46
2.7.3. Density function theory (DFT) based theoretical calculations.....	46
2.7.4. Principal component analysis (PCA) technique for statistical analysis .....	47
2.8. Summary .....	49

**CHAPTER 3: AG NANOSTRUCTURE-BASED SERS DETECTION, CLINICAL STUDY, QUANTIFICATION AND DISEASE PROGNOSIS OF HIV..... 50**

<i>PART A. Portable and sensitive Ag nanorods SERS platform for HIV detection and tropism determination .....</i>	<i>51</i>
3.A.1. Introduction.....	51
3.A.2. Materials and Methods.....	53
3.A.2.2. Cells and viruses .....	53
3.A.2.3. SERS Measurements.....	54
3.A.2.4. Statistical classification and analysis .....	55
3.A.3. Results and Discussion .....	55
3.A.3.1. Fabrication and characterization of SERS substrates .....	55
3.A.3.2. Determination of range of detection in SERS platform for different HIV-1 subtypes spiked in diethylpyrocarbonate (DEPC) treated water .....	57
3.A.3.3. SERS peak intensity-based statistical study and outcomes .....	60
3.A.3.4. Assignment and comparison of peaks.....	61
3.A.3.5. Peak variation in Subtype D HIV-1 virus.....	63
3.A.3.6. Detection of HIV-1 subtypes spiked in healthy plasma using SERS platform.....	63
3.A.3.7. Multivariate data analysis and classification .....	66
3.A.4. Conclusions.....	67
<i>PART B. CLINICAL STUDY OF HIV-1 VIRAL LOAD QUANTIFICATION AND DETERMINATION OF DISEASE PROGNOSIS USING THE DEVELOPED SERS PLATFORM.....</i>	<i>68</i>

3.B.1.	Introduction.....	68
3.B.2.	Materials and Methods.....	71
3.B.2.1.	Clinical samples used for determining the HIV-1 viral load.....	71
3.B.2.2.	HIV-1 strains used for determining the tropism .....	71
3.B.2.3.	Fabrication of SERS substrates and SERS measurements .....	72
3.B.2.4.	RCWA simulations and statistical analysis.....	74
3.B.3.	Results and Discussions .....	75
3.B.3.1.	Characterization of SERS substrates.....	75
3.B.3.2.	Efficacy of SERS platform in measuring HIV-1 viral load / detection .....	76
3.B.3.3.	Efficacy of SERS platform in determining HIV-1 tropism .....	78
3.B.3.4.	RCWA simulations and PCA analysis.....	82
3.B.4.	Conclusion .....	84
<b>CHAPTER 4:HIGHLY SENSITIVE M-SERS SENSING OF HEMOZOIN AND ITS SEPARATION FROM CO-INFECTIONS USING UTLC-SERS PLATFORM.....</b>		<b>85</b>
PART A. HIGHLY SENSITIVE GLAD BASED MAGNETIC SERS SENSING OF HEMOZOIN BIOMARKER FOR RAPID MALARIA DIAGNOSIS .....		86
4.A.1.	Introduction.....	86
4.A.2.	Experimental details.....	88
4.A.2.1.	Reagents.....	88
4.A.2.2.	Magnet substrates .....	88
4.A.2.3.	Fabrication of Ag nanorods .....	88
4.A.2.4.	Characterization of SERS substrates and hemozoin crystals.....	89
4.A.2.5.	SERS measurements .....	90
4.A.3.	Results and discussion .....	90
4.A.3.1.	Magnetic SERS substrate fabrication and characterization .....	90
4.A.3.2.	Magnetic properties of hemozoin.....	92
4.A.3.3.	SERS measurements for Hz and Hg .....	95
4.A.4.	Conclusions.....	102
PART B: MAGNETIC FIELD AUGMENTED UTLC- SERS DETECTION AND SEPARATION OF HEMOZOIN FROM BACTERIAL MIXTURE.....		104
4.B.1.	Introduction .....	104

4.B.2. Materials and methods.....	106
4.B.2.1. Reagents .....	106
4.B.2.2. Fabrication of Ag nanorods based UTLC-SERS substrates.....	106
4.B.2.3. Culture of bacterial strains.....	107
4.B.2.4. Staining of bacteria and hemozoin .....	107
4.B.2.5. UTLC process .....	108
4.B.2.6. SERS measurement, characterization and data analysis.....	108
4.B.3. Results and discussion .....	109
4.B.3.1. SERS spectra of individual components.....	109
4.B.3.2. UTLC development for the bacterial and hemozoin mixture .....	112
4.B.3.3. UTLC development for the bacterial and hemozoin mixture after staining .....	117
4.B.4. Conclusion .....	121
4.B.5. Benchmark in tabular form showing comparison of present techniques for malaria detection with the prescribed SERS based GLAD detection.....	122
<b>CHAPTER 5: ULTRA-SENSITIVE PLASMONIC CHIRAL SERS SUBSTRATE FOR LABEL-FREE ENATIO-SELECTIVE DISCRIMINATION .....</b>	<b>124</b>
5.1. Introduction.....	125
5.2. Experimental techniques .....	127
5.2.1. Reagents .....	127
5.2.2. Fabrication of chiral SERS substrates.....	128
5.2.3. Characterization of chiral SERS substrates.....	129
5.2.4. SERS measurements.....	129
5.2.5. Finite difference time domain (FDTD) simulations .....	130
5.3. Results and discussion .....	130
5.3.1. Fabrication and characterization of chiral SERS substrates.....	130
5.3.2. SERS measurements for the enantiomers.....	132
5.3.3. Proposed mechanisms for SERS discrimination using the chiral substrates .....	138
5.4. Conclusions.....	143

<b>CHAPTER 6: CONCLUSION AND SCOPE FOR FUTURE STUDY .....</b>	<b>144</b>
6.1. Summary of the present thesis .....	145
6.2. Scope of future studies.....	147
<b>BIBLIOGRAPHY .....</b>	<b>148</b>
<b>PUBLICATIONS .....</b>	<b>184</b>
<b>BIODATA.....</b>	<b>184</b>

## LIST OF FIGURES

---

<b>Figure 1.1</b>	: Jablonski diagram for the Rayleigh and the Raman scattering quantum energy transitions <sup>56</sup> .....8	8
<b>Figure 1.2</b>	: Schematic diagram explaining the concept of electromagnetic (EM) SERS enhancement.....12	12
<b>Figure 1.3</b>	: Schematic diagram showing the process of the electromagnetic enhancement as (a) Collective oscillations of conductive metallic electrons resulting into highly localized EM fields when irradiated with light <sup>66</sup> , (b) The electromagnetic ‘hotspot’ in gap between the 2 Ag nanoparticles enhancing the local EM field experienced by the analyte.....14	14
<b>Figure 1.4</b>	: Schematic showing (a) chemical enhancement due to the electron transfer between molecule and the metallic nanoparticles. <sup>72</sup> (b) Four-step process of photon-imitated charge transfer mechanism for a molecule adsorbed on a metallic surface.....16	16
<b>Figure 1.5</b>	: (a) Schematic diagram of GLAD set-up where $\alpha$ is the angle subtended by the incoming vapor flux with the substrate normal and $\phi$ is azimuthal angle (b) Step by step mechanistic view of GLAD based columnar growth (i) Incoming vapor flux at an angle $\alpha$ resulting into the random nucleation at the substrate (ii) Nuclei growth casting neighbouring shadow as shown by the dotted lines (iii) Columns growth suppressing the neighbour’s growth by the shadowing effect (iv) Full column growth at a specific angle ( $\beta$ ) with respect to the substrate normal. ....22	22
<b>Figure 1.6</b>	: Various fabricated GLAD-structured thin films. (a) Slanted films; (b) chevron (zig-zag) films with 4 arms; (c) AgNR/SiO <sub>2</sub> SCL/SiO <sub>2</sub> /PCL/Ag multilayer nanostructured	

	substrates; (d) helical or spring film; (e) vertical post structure; (f) 45° tilted top view of fabricated Au mushrooms .....26
<b>Figure 2.1</b>	: Schematic diagram showing the initial formation of the nucleation centres and the shadowing effect.....35
<b>Figure 2.2</b>	: (a) Schematic showing working of GLAD technique (b) Digital photograph of homemade customized GLAD setup with fixed substrate angle ( $\alpha$ ).....36
<b>Figure 2.4</b>	: (a) Digital photograph of advanced GLAD setup equipped with multi-axis positioning system unit for the variation of $\alpha$ and $\phi$ angles of substrate. (b) The UHV compatible multi axis positioning system unit (c) zoomed view of the thermal/GLAD configuration.....38
<b>Figure 2.5</b>	: (a) Digital photograph of the substrate packaging unit procured in class 1000 cleanroom (b) Packed SERS substrates in a slide mailer using inert N <sub>2</sub> gas .....39
<b>Figure 2.6</b>	: (a) Schematic showing X-Ray diffraction process <sup>136</sup> (b) Digital image of Panalytical Xpert powder diffractometerNARI .....40
<b>Figure 2.7</b>	: (a) Schematic of Field emission electron microscopy <sup>137</sup> (b) Photograph of JEOL JSM 7800 Prime FESEM under CRF IIT Delhi .....41
<b>Figure 2.8</b>	: (a) Schematic of Transmission electron microscopy (TEM) <sup>138</sup> (b) Photograph of JEOL JAM 1400 microscope.....42
<b>Figure 2.9</b>	: (a) Schematic showing AFM working <sup>139</sup> (b) Bruker Dimension Icon AFM picture used in present work.....43
<b>Figure 2.10</b>	: (a) Schematic instrumentation of Raman spectrometer <sup>143</sup> (b) Photograph of Renishaw inVia Raman spectrometer used in the present work .....44
<b>Figure 2.11</b>	: Photograph of TSI USA handheld portable Raman spectrometer .....45
<b>Figure 3.1</b>	: Schematic diagram demonstrating rapid handheld SERS platform for HIV detection.....53

<b>Figure 3.2</b>	: The characterization of SERS substrates AgNRs array.....	56
<b>Figure 3.3</b>	: (a) Comparison of SERS signal of BPE and bare AgNRs array respectively for determining SERS enhancement factor (Each plot is average of two different spectra obtained from different substrates which are the further average of six spectra obtained from different spots of the same substrate) (b) Plot of SERS peak intensity (1635 cm <sup>-1</sup> ) against BPE concentrations.....	57
<b>Figure 3.4</b>	: Subtype C (HIV-1 VB51) spiked in PBS concentrated on different gradients ( sucrose, CsCl, histopaque) at conc. 2x10 <sup>5</sup> cp/ml.....	59
<b>Figure 3.5</b>	: Signature peaks obtained on the SERS platform for HIV-1 spiked in DEPC treated water. (a) The signature peaks of 5 different viral subtypes in DEPC treated water at conc. 2×10 <sup>5</sup> copies/mL (b) VB51 spectra for all the concentrations of virus prepared in DEPC treated water showing good reproducibility. ....	59
<b>Figure 3.6</b>	: Graphical analysis to determine the relationship between the concentration of virus (copies/mL) and intensity of peaks. ....	60
<b>Figure 3.7</b>	: (a) Spectra of varying concentration of HIV-1UG070 spiked in DEPC treated water (b) Similar spectra obtained for the X4 tropic viruses UG070 and pNL 4.3 viral strains.....	63
<b>Figure 3.8</b>	: Signature peaks obtained on SERS platform for HIV-1 spiked in plasms (a) Signature peaks of five different virus subtypes spiked in healthy plasma (conc. 2×10 <sup>5</sup> cp/ml) (b) Signature peaks of subtype D virus spiked in plasma (undiluted plasma) and signature peaks of subtype D virus spiked in DEPC treated water (conc. 10 <sup>5</sup> cp/ml) (c) Comparison between the spectra of healthy plasma (control) and subtype D virus spiked in plasma .....	64
<b>Figure 3.9</b>	: (a) Signature peaks for HIV-1UG070 spiked in healthy plasma (1:20 diluted in PBS) (b) Signature peaks for HIV-1UG070	

	spiked in healthy plasma (1:50 diluted in PBS) (c) Comparison between spectra of control plasma and virus spiked in healthy plasma (1:20 dilution in PBS) (d) Comparison between spectra of control plasma and virus spiked in healthy plasma (1:50 dilution in PBS).....	65
<b>Figure 3.10</b>	: (a) Signature peaks Virus (UG070) infected serum (1:20 diluted) (b) Comparison between spectra of serum (control) and virus-infected serum .....	66
<b>Figure 3.11</b>	: PCA for HIV-1 spectra (a) PC scatter plot for plasma samples (b) PC1 loading of 7(a) vs. Raman shift (c) PC scatter plot for different HIV-1 strains in plasma (d) PC scatter for different HIV-1 strains in DEPC treated water .....	67
<b>Figure 3.12</b>	: (a) Schematic showing SERS measurements for HIV-1 clinical samples taken over three different GLAD fabricated substrates using handheld Raman spectrometer. (b) Co-receptor tropism (X-4 tropic, R-5 tropic and dual tropic) of HIV-1 showing their affinity towards specific co-receptors .....	70
<b>Figure 3.13</b>	: Comparison of SERS spectra of BPE taken over 3 different substrates respectively. ....	73
<b>Figure 3.14</b>	: FESEM images of (a) 1 arm AgNRs array. The inset show cross sectional image of the same. (b) 2 arm AgNRs array (c) Au sputtered AgNRs array with inset showing crosssectional view of the same. EDX spectra of (d) AgNRs array (e) Au sputtered AgNRs array .....	75
<b>Figure 3.16</b>	: SERS spectra of X-4 tropic and R-5 tropic strains for (a) subtype A (b) Subtype B (c) Subtype C (d) Subtype D respectively. Each of these spectra are an average of 10 different spectra and are baseline corrected. Comparison of SERS spectra of Subtype C R5 tropic strain for (e) Au sputtered AgNRs, 2 arm AgNRs, 1 arm AgNRs respectively for $10^5$ cp/ml (f) Au sputtered AgNRS and 1 arm AgNRs for $10^5$ cp/ml and 100 cp/ml respectively. Subtype C X4 tropic	

	strain for (g) Au sputtered AgNRs, 2 arm AgNRs, 1 arm AgNRs respectively for $10^5$ cp/ml (h) Au sputtered AgNRs and 1 arm AgNRs for $10^5$ cp/ml and 100 cp/ml, respectively. ....	79
<b>Figure 3.17</b>	: The SERS spectra of different HIV-1 subtypes for (a) R5 tropic strains (b) X4 tropic strains. Each data plot is an average of 6 different spectra over 2 substrates. ....	81
<b>Figure 3.18</b>	: (a) SERS spectra of the dual tropic strains (b) Comparison of the SERS spectra of dual tropic strain with R5 tropic and X4 tropic respectively.....	82
<b>Figure 3.19</b>	: RCWA simulations showing electric field distribution for (a) single arm AgNRs (b) 2 arm AgNRs (c) Au sputtered AgNRs (d) Material index profile of Au scattered AgNRs. PCA scatter plot for (c) HIV-1 plasma samples of 7 different ranges of viral load (d) HIV-1 samples for different subtypes classified on the basis of their tropism .....	83
<b>Figure 4.1</b>	: SEM images of GLAD deposited AgNRs over glass substrates at (a) room temperature (300 K) and (b) at 120 K substrate temperature. (c) XRD pattern for these AgNRs SERS substrates. (d) Comparison of Raman and SERS spectra of BPE analyte over c-SERS, M-SERS substrates and on 200 nm thin Ag film. ....	92
<b>Figure 4.2</b>	: M-H measurement curve for (a) Hz after 0.3T magnetic field treatment, (b) unmagnetized Hz, (c) Hb after 0.3T magnetization, and (d) unmagnetized Hb.....	93
<b>Figure 4.4</b>	: FESEM images of Hz crystals (a) randomly oriented on tilted Ag nanorods surface and (b) agglomerated over Ag tilted nanorods after application of 0.3 T applied magnetic field.....	95
<b>Figure 4.5</b>	: Comparison of SERS spectra for (a) hemozoinon Ag nanorods arrays fabricated on glass ( $H_{zg}$ ), neodymium magnet ( $H_{zm}$ ), $H_{zg}$ substrate kept under 0.3T external magnetic field for 1 hour ( $H_{zex}$ ), and (b) hemoglobin on Ag nanorods arrays fabricated on glass ( $H_{bg}$ ), neodymium	

	magnet ( $H_{b_m}$ ), $H_{b_g}$ substrate kept under 0.3 T external magnetic field for 1 hour ( $H_{b_{ex}}$ ).....	96
<b>Figure 4.6</b>	: (a) Comparative SERS spectra of $H_{z_m}$ , $H_{z_g}$ , $H_{b_m}$ and $H_{b_g}$ respectively for all the substrates grown at low temperature (120K) conditions. (b) Variation of SERS signal intensity for $1620\text{ cm}^{-1}$ peak with the applied magnetic field for $H_{z_m}$ and $H_{b_m}$ .....	97
<b>Figure 4.7</b>	: Schematic diagram showing (a) pyridine- AgNRs interaction for unmagnetized Hz over AgNRs SERS substrate (c-SERS) (b) effective pyridine – AgNRs interaction for Hz in the vicinity of magnetic field (M-SERS). (c) pyridine- AgNRs interaction for unmagnetized Hg over AgNRs SERS substrate (c-SERS) (d) effective pyridine – AgNRs interaction for Hg in the vicinity of magnetic field (M-SERS). (e) RCWA modelling to show localized hotspots in the nanorods gap for effective hotspot-analyte interaction .....	99
<b>Figure 4.8</b>	: Conc. vs Intensity graph for (a) $H_{z_g}$ and $H_{z_m}$ , (b) $H_{b_g}$ and $H_{b_m}$ respectively for $1620\text{ cm}^{-1}$ peak (c) RSD values obtained $H_{z_m}$ and $H_{z_g}$ corresponding to $1620\text{ cm}^{-1}$ peak. (d) RSD values obtained for $H_{b_m}$ and $H_{b_g}$ corresponding to $1620\text{ cm}^{-1}$ peak.....	100
<b>Figure 4.10</b>	: SERS spectral intensity comparison at different dilutions for (a) $H_{z_{ex}}$ (M-SERS) (b) $H_{z_g}$ (c-SERS) (c) $H_{b_{ex}}$ (M-SERS) (d) $H_{b_g}$ (c-SERS). .....	101
<b>Figure 4.11</b>	: Comparison of SERS spectra for (a) hemozoin in FBS on Ag nanorods arrays fabricated on glass ( $H_z$ in FBS) <sub>g</sub> neodymium magnet ( $H_z$ in FBS) <sub>m</sub> , ( $H_z$ in FBS) <sub>g</sub> substrate kept under 0.3T external magnetic field for 1 hour ( $H_z$ in FBS) <sub>ex</sub> , and (b) hemoglobin in FBS on Ag nanorods arrays fabricated on glass ( $H_b$ in FBS) <sub>g</sub> , neodymium magnet ( $H_b$ in FBS) <sub>m</sub> , $H_{b_g}$ substrate kept under 0.3 T external magnetic field for 1 hour ( $H_b$ in FBS) <sub>ex</sub> . (c) PCA analysis for Hg in FBS and Hz in FBS .....	102

<b>Figure 4.12</b>	: Schematic diagram showing steps involved in (a) Fabrication of AgNRs using GLAD technique (b) Magnetic field based UTLC-SERS separation of hemozoin from bacterial mixtures .....	109
<b>Figure 4.13</b>	: (a) SERS spectra of hemozoin (Hz), <i>P. aeruginosa</i> (PA), <i>S. aureus</i> (SA) (b) SERS spectra of mixture of PA, SA and Hz; SA and Hz; PA and Hz (c) SERS spectra of 3 stained SA, PA and Hz (d) SERS spectra of stained Hz + stained PA + stained SA; stained Hz + stained SA; stained Hz + stained PA, respectively.....	110
<b>Figure 4.14</b>	: SERS spectra after UTLC flow taken for (a) <i>P.A.</i> (Gram - negative bacteria) and hemozoin mixture (b) <i>S.A.</i> (Gram - positive) and hemozoin mixture (c) PA, SA and Hz mixture .....	113
<b>Figure 4.15:</b>	(a) SERS spectra after UTLC development for SA, PA and Hz mixture without application of external magnetic field. (b) SERS spectra after UTLC development for SA and PA mixture without application of external magnetic field .....	114
<b>Figure 4.16</b>	: Normalized intensity vs distance curve for the signature peaks for (a) PA and Hz mixture (b) SA and Hz mixture (c) PA, SA and Hz mixture (d) Histograms showing comparison of retention factor values for the 3 mixtures after UTLC development .....	116
<b>Figure 4.17</b>	: FESEM images of mixture of PA-Hz (a) before flow at the mixture loaded area (b) after flow around 4mm area (c) after flow around 9 mm area; mixture of SA-Hz (d) before flow at the loaded area (e) after flow around 4 mm area (f) after flow around 9 mm area; mixture of PA, SA and Hz (g) before flow at the mixture loaded area (h) after flow around 4mm area (i) after flow around 9 mm area .....	117
<b>Figure 4.18</b>	: Fluorescence images of stained (a) PA using acridine orange (b) SA using rhodamine 6G.....	117

<b>Figure 4.19</b>	: SERS spectra after UTLC flow taken for (a) Acridine orange-stained PA and methylene blue stained Hz mixture (b) Rhodamine 6G stained SA and methylene blue stained Hz (c) mixture of acridine orange-stained PA, rhodamine 6G stained SA and methylene blue stained Hz respectively .....	118
<b>Figure 4.20</b>	: Normalized intensity vs distance curve for the signature peaks for (a) acridine orange-stained PA and methylene blue stained Hz mixture (B) rhodamine 6G stained SA and methylene blue stained Hz mixture (c) stained PA, stained SA and stained Hz mixture (d) Histograms showing comparison of retention factor values for the 3 mixtures after UTLC development. AO, RG and MB are the acronyms used for acridine orange, rhodamine 6G and methylene blue respectively .....	119
<b>Figure 4.21</b>	: (a) Digital picture of AgNRs based UTLC-SERS plate after the flow for mixture of 3 stained components with descriptions marked (b) RGB performed using the colour coding of the digital picture of the UTLC-SERS plate separating the 3 dyes individually .....	120
<b>Figure 5.1</b>	: The chemical structure and CD spectra of (a) DOPA (b) cystine (c) tartaric acid respectively. Here, the in-plane and out of plane spatial arrangements are shown by usual symbols. ....	128
<b>Figure 5.4</b>	: SERS data taken over AgNRs for (a) L/D-DOPA (b) L/D-cystine (c) L/D- tartaric acid .....	132
<b>Figure 5.8</b>	: Side view (Y-Z) and top view (x-Y) of FDTD simulation results showing the chiral field pattern for (a) (-)-AgNHs (b) (+)-AgNHs .....	139
<b>Figure 5.9</b>	: Energy level diagram of the (a) Ag-L-DOPA complex assembly (b) Ag-D-DOPA complex assembly 3-D visualization of theoretically modelled (c) HOMO-LUMO energies of L-DOPA (d) HOMO-LUMO energies of D-DOPA .....	140

<b>Figure 5.10</b>	: Energy level diagram of the (a) Ag-L-cystine complex assembly (b) Ag-D-cystine complex assembly (c) HOMO-LUMO energies of L-cystine (d) HOMO-LUMO energies of D- cysteine.....	141
<b>Figure 5.11</b>	: Energy level diagram of the (a) Ag-L-tartaric acid complex assembly (b) Ag-D- tartaric acid complex assembly (c) HOMO-LUMO energies of L-tartaric acid (d) HOMO-LUMO energies of D- tartaric acid .....	141
<b>Figure 5.12</b>	: Comparative flow chart showing the gap of Ag fermi level from the the HOMO-LUMO energy levels of the different enantiomers. ....	142

## LIST OF TABLES

---

<b>Table 1.1</b>	: Various periodic nanostructures formed using different combinations of $\alpha$ and $\phi$ in GLAD setup .....	24
<b>Table 3.1</b>	: Peak assignment and comparison for virus spiked in plasma and DEPC treated water, respectively. * represents the most prominent peaks for HIV-1 with notable variations, ** represents the peaks unique to subtype D (X4 tropic).....	62
<b>Table 3.4</b>	: Plasma samples in different viral load ranges selected for HIV-1 detection using SERS platform .....	71
<b>Table 3.5</b>	: HIV-1 strains selected for determining the tropism using SERS platform .....	72
<b>Table 3.6</b>	: The calculated constant ratio of the peaks with increasing intensity and decreasing intensity providing a quantitative correlation between the peaks. ....	77
<b>Table 3.7</b>	: Peak assignment and comparison for HIV-1 clinical samples and HIV-1 samples for different subtypes classified on the basis of their tropism.* represents the peak which are unique to subtype D (x4 tropic) .....	80
<b>Table 4.1</b>	: Raman peak assignment for hemozoin and hemoglobin.....	97
<b>Table 4.2</b>	: Peak assignment for <i>P. aruginosa</i> , <i>S. aureus</i> and hemozoin respectively.....	110
<b>Table 4.3</b>	: Peak assignment for acridine orange, rhodamine 6G and methylene blue respectively .....	111
<b>Table 4.4</b>	: Retention factor of signature peaks for each component of 3 different mixtures after UTLC development.....	115
<b>Table 4.5</b>	: Comparison of SERS platform for malaria detection with other exiting techniques.....	122
<b>Table 5.1</b>	: SERS enhancement factor for various GLAD fabricated SERS substrates .....	132

<b>Table 5.2</b> : Peak assignment for DOPA, cystine and tartaric acid.....	133
<b>Table 5.4</b> : HOMO-LUMO energy level values and gap of LUMO from Ag fermi level obtained for DOPA, cystine and tartaric acid enantiomers .....	142

## SYMBOLS

---

$\nu_{\text{vib}}$	Vibrational frequency of a molecule
$\mu$	Magnitude of induced dipole moment
$\alpha$	Polarizability of a molecule
$\beta$	Inclination of nano-columns
$\sigma_{\text{RS}}$	Raman scattering cross section
$\text{\AA}$	Angstrom
$E$	Electric field
$E_a$	Energy barrier of the diffusion process
$E_{\text{rad}}$	Radiated electric field
$I_e$	Excitation light intensity
$k_b$	Boltzmann's constant
$P_s(\nu_s)$	Power of the scattered beam
$N$	Number of Raman active scatterers
$I(\nu_L)$	Intensity of the excitation light beam
$L(\nu)$	Enhancement factor for the scattered field
$\epsilon_0$	Dielectric constant
$G_{\text{em}}(\nu_s)$	Stokes signal power
$\epsilon(\nu)$	Dielectric constant of metal sphere
$\Phi$	Azimuthal substrate rotation
$\gamma$	Sweep angle
$T_m$	Melting temperature
$T_s$	Substrate temperature
$D$	Molecule diffusion coefficient
$\omega_p$	Volume/bulk plasma frequency
$\omega_{\text{sp}}$	Surface plamon frequency
$\frac{d\sigma}{d\Omega}$	Solid angle
$\text{eV}$	Electron Volt

## ABBREVIATIONS

---

AFM	Atomic force microscope
AgNHs	Silver nanohelices
AgNRs	Silver nanorods
AIDS	Acquired immunodeficiency syndrome
AO	Acrydine orange
BPE	1, 2 bis (4-pyridyl)-ethylene
CD	Circular dichroism
CE	Chemical enhancement
c-SERS	Conventional-SERS
CT	Charge transfer
DEPC	Diethylene pyrocarbonate
DFT	Density function theory
DOPA	1-3-(3,4-dihydroxyphenyl) alanine
EBL	Electron beam lithography
ELISA	Enzyme linked immunosorbent assay
EME	Electromagnetic enhancement
FDTD	Finite-difference time – domain
FE-SEM	Field emission scanning electron microscopy
FRET	Fluorescence resonance-based energy transfer
GC-SERS	Gas chromatography-surface-enhanced Raman scattering
Gp120	Glycoprotein 120
GLAD	Glancing angle deposition
Hb	Hemoglobin
HIV	Human immunodeficiency virus

Hz	Hemozoin
HR-TEM	High resolution transmission electron microscopy
HOMO	Highest occupied molecular orbital
LOD	Limit of detection
LSPR	Localized surface plasmon resonance
LUMO	Lowest unoccupied molecular orbital
MB	Methylene blue
M-SERS	Magnetic SERS
NIH	National Institutes of Health
OAD	Oblique angle deposition
PA	<i>Pseudomonas aeruginosa</i>
PBMCs	Peripheral blood mononuclear cells
PBS	Phosphate-buffered saline
PCA	Principal component analysis
PCR	Polymerase chain reaction
PSPs	Propagating surface plasmons
PVD	Physical vapor deposition
RBCs	Red blood cells
RCWA	Rigorous coupled wave analysis
RDTs	Rapid diagnostic tools
R6G	Rhodamine 6G
RRS	Resonant Raman scattering
RSD	Relative standard deviation
SA	<i>Staphylococcus aureus</i>
SERS	Surface enhanced Raman spectroscopy

SEHRS	Surface-enhanced hyper-Raman spectroscopy
SEROA	Surface enhanced Raman optical activity
SPR	Surface plasmon resonance
TEM	Transmission electron microscope
TERS	Tip enhanced Raman spectroscopy
UHV	Ultra-high vacuum
UTLC	Ultra-thin layer chromatography
XRD	X-ray diffraction